Inorg. Chem. **2008**, *47*, 5365−5371

Covalency Trends in Group IV Metallocene Dichlorides. Chlorine K-Edge X-Ray Absorption Spectroscopy and Time Dependent-Density Functional Theory

Stosh A. Kozimor, Ping Yang, Enrique R. Batista, Kevin S. Boland, Carol J. Burns, Christin N. Christensen, David L. Clark,* Steven D. Conradson,* P. Jeffrey Hay, Juan S. Lezama, Richard L. Martin,* Daniel E. Schwarz, Marianne P. Wilkerson, and Laura E. Wolfsberg

Los Alamos National Laboratory, Los Alamos, New Mexico 87545

Received March 18, 2008

For 3−5d transition-metal ions, the $(C_5R_5)_2MCl_2$ (R = H, Me for M = Ti, Zr, Hf) bent metallocenes represent a series of compounds that have been central in the development of organometallic chemistry and homogeneous catalysis. Here, we evaluate how changes in the principal quantum number for the group IV $(C_5H_5)_2MCl_2$ (M = Ti, Zr, Hf; **1**−**3**, respectively) complexes affects the covalency of M−Cl bonds through application of Cl K-edge X-ray Absorption Spectroscopy (XAS). Spectra were recorded on solid samples dispersed as a thin film and encapsulated in polystyrene matrices to reliably minimize problems associated with X-ray self-absorption. The data show that XAS pre-edge intensities can be quantitatively reproduced when analytes are encapsulated in polystyrene. Cl K-edge XAS data show that covalency in M−Cl bonding changes in the order Ti > Zr > Hf and demonstrates that covalency slightly decreases with increasing principal quantum number in **1**−**3**. The percent Cl 3p character was experimentally determined to be 26, 23, and 18% per M−Cl bond in the thin-film samples for **1**−**3** respectively and was indistinguishable from the polystyrene samples, which analyzed as 25, 25, and 19% for **1**−**3**, respectively. To aid in interpretation of Cl K-edge XAS, **1**−**3** were also analyzed by ground-state and time-dependent density functional theory (TD-DFT) calculations. The calculated spectra and percent chlorine character are in close agreement with the experimental observations, and show 20, 18, and 17% Cl 3p character per M−Cl bond for **1**−**3**, respectively. Polystyrene matrix encapsulation affords a convenient method to safely contain radioactive samples to extend our studies to include actinide elements, where both 5f and 6d orbitals are expected to play a role in M−Cl bonding and where transition assignments must rely on accurate theoretical calculations.

Introduction

The bent metallocenes of the general formula $(C_5R_5)_2MX_2$ (R = H, CH_3; X = monoanion) represent a series of complexes with similar molecular structures for transition metals[1−7] (groups IV, V, VI) and light actinides (Th,[8,9] U,[8,9] and Np[10]) and are among the most extensively utilized systems in organometallic research.[11−13] Theoretical and spectroscopic studies of metallocenes indicate that variations

* To whom correspondence should be addressed. E-mail: dlclark@lanl.gov.

(1) Wilkinson, G.; Birmingham, J. M. *J. Am. Chem. Soc.* **1954**, *76*, 4281.
(2) Brainina, E. M.; Freidlina, R. Kh.; Minacheva, M. Kh., *Dolkady Akad. Nauk S. S. S. R.* **1967**, *173*, 581.
(3) *Organometallic Syntheses* Eisch, J. J., King, R. B., Eds.; Academic Press: New York, 1967; Vol. 1, p 75.
(4) Druce, P. M.; Kingston, B. M.; Lappert, M. F.; Spalding, T. R.; Srivastava, R. C. *J. Chem. Soc. A* **1969**, 2106.
(5) Bercaw, J. E. *J. Am. Chem. Soc.* **1974**, *96*, 5087.
(6) Manriquez, J. M.; McAlister, D. R.; Rosenberg, E.; Shiller, A. M.; Williamson, K. L.; Chan, S. I.; Bercaw, J. E. *J. Am. Chem. Soc.* **1978**, *100*, 3078.
(7) Roddick, D. M.; Fryzuk, M. D.; Seidler, P. F.; Hillhouse, G. L.; Bercaw, J. E. *Organometallics* **1985**, *1*, 97.
(8) Manriquez, J. M.; Fagan, P. J.; Marks, T. J.; Vollmer, S. H.; Day, C. S.; Day, V. W. *J. Am. Chem. Soc.* **1979**, *101*, 5075.
(9) Fagan, P. J.; Manriquez, J. M.; Maatta, E. A.; Seyam, A. M.; Marks, T. J. *J. Am. Chem. Soc.* **1981**, *103*, 6650.
(10) Sonnenberger, D. C.; Gaudiello, J. *J. Less-Common. Met.* **1986**, *126*, 411.
(11) Qian, Y.; Huang, J.; Bala, M. D.; Lian, B.; Zhang, H.; Zhang, H. *Chem. Rev.* **2003**, *103*, 2633.
(12) Alt, H. G.; Koppl, A. *Chem. Rev.* **2006**, *100*, 1205.
(13) Mohring, P. C.; Coville, N. J. *Coord. Chem. Rev.* **2006**, *250*, 18.
(14) Fragalá, I.; Marks, T. J.; Fagan, P. J.; Manriquez, J. M. *; J. Electron Spectrosc. Relat. Phenom.* **1980**, *20*, 249.
(15) Ciliberto, E.; Condorelli, G.; Fagan, P. J.; Manriquez, J. M.; Fragalá, I.; Marks, T. J. *J. Am. Chem. Soc.* **1981**, *103*, 4755.

10.1021/ic8004932 CCC: $40.75
Published on Web 05/10/2008

Scheme 1

M = Ti, Zr, Hf **M = Ti, Zr, Hf, Th, U, Np**

in orbital character and metal d and f covalency are connected with differences in chemical reactivity.[14–24] Of the experimental approaches to determine covalency, ligand K-edge X-ray Absorption Spectroscopy (XAS) has emerged as a powerful measure of the amount of ligand orbital mixing with metal-based orbitals.[25–37] On the low-energy side of the ligand K-edge are bound-state transitions of ligand 1s electrons into metal-based orbitals that contain ligand p character due to covalent mixing. The intensity of these pre-edge features provides a direct experimental measure of covalency.[30,31]

Because the $(C_5R_5)_2MCl_2$ (R = H, CH_3) series for transition metals and light actinides are structurally similar (Scheme 1), they are well-suited for a ligand K-edge XAS study to compare relative changes in orbital mixing between a common Cl^{1-} ligand and 3d, 4d, 5d, and 6d/5f orbitals in metal−ligand bonding. Moreover, their electronic structure is well understood,[38–43] and the Cl K-edge XAS of the first member of this series, $(C_5H_5)_2TiCl_2$, has been recently analyzed by experiment and theory,[32,44] thereby providing a standard for comparison with heavier congeners.

Herein, we report a comparison of Cl K-edge XAS of group IV $(C_5H_5)_2MCl_2$ complexes (M = Ti, Zr, and Hf; **1**, **2**, and **3**, respectively) recorded as thin films and encapsulated in polystyrene. The latter is developed as a new protocol for containment of radioactive samples in ligand K-edge XAS studies. We also employ time dependent-density functional theory (TD-DFT) to aid assignments of ligand XAS features[44–47] and provide further insight into the electronic structure.

Experimental Section

General Considerations. The manipulations of the following compounds and samples were conducted under helium with exclusion of air and water by Schlenk, glovebox, and glovebag techniques. Toluene was distilled over sodium and benzophenone and degassed by three freeze−pump−thaw cycles. Polystyrene (PolySciences Inc.) was acquired as 3.0 Micron Dry Form and dried under vacuum (10^{-3} Torr) for 24 h. The polystyrene was verified to contain no chlorine by Cl K-edge X-ray absorption spectroscopy. The D_{2d}−Cs_2CuCl_4 intensity and energy calibration standard was prepared as previously described.[48] The $(C_5H_5)_2MCl_2$ (M = Ti, Zr, and Hf; **1**, **2**, and **3**, respectively) compounds were obtained from Aldrich and recrystallized from solutions of hot toluene, and their purity was confirmed by ^1H NMR spectroscopy before use.[4]

Thin Film Sample Preparation. Thin film samples were prepared by adhering Kapton tape, which was determined to be free of chlorine by Cl K-edge XAS, to one side of a stainless steel sample holder that contained 2 × 10 mm slots. The analyte was ground for 10 min with a mortar and pestle to produce a fine powder and dispersed as thinly as possible in the sample holder slot on the Kapton tape using Ultrafine (#1) synthetic fiber artist's brushes. The open side of the sample plate was sealed with a 4.5 μm polypropylene film.

Polystyrene Sample Preparation. The polystyrene samples, which contained **1**−**3** (0.8% by mass) encapsulated in polystyrene matrices, were prepared by adding a solution that contained finely ground $(C_5H_5)_2MCl_2$ (0.7 mg) in toluene (100 μL) to a solution of polystyrene (90 mg) and toluene (300 μL). The resulting solution was transferred to a 4 × 10 mm slot in an aluminum sample plate,

(16) Ciliberto, E.; Di Bela, S.; Gulino, A.; Fragalá, I.; Petersen, J. L.; Marks, T. J. *Organometallics* **1992**, *11*, 1727.
(17) Green, J. C. *Chem. Soc. Rev.* **1998**, *27*, 263.
(18) King, W. A.; Di Bella, S.; Gulino, A.; Zanza, G.; Fragalá, Stern, C. L.; Marks, T. J. *J. Am. Chem. Soc.* **1999**, *121*, 355.
(19) Di Bell, S.; Lanza, G.; Fragalá, I. L.; Marks, T. J. *Organometallics* **1996**, *15*, 205.
(20) Zachmanoglou, C. E.; Docrat, A.; Bridgewater, B. M.; Parkin, G.; Brandow, C. G.; Bercaw, J. E.; Jardine, C. N.; Lyall, M.; Green, J. C.; Keister, J. B. *J. Am. Chem. Soc.* **2002**, *124*, 9525.
(21) Wang, X.; Chen, L.; Endou, A.; Kubo, M.; Miyamoto, A. *J. Organomet. Chem.* **2003**, *678*, 156.
(22) Clark, J. P.; Green, J. C. *J. Less-Common Met.* **1977**, *54*, 63.
(23) Petersen, J. L.; Lichtenberger, D. L.; Fenske, R. F.; Dahl, L. F. *J. Am. Chem. Soc.* **1975**, *97*, 6433.
(24) Condorelli, F.; Fragala, I.; Centineo, A.; Tondello, E. *J. Organomet. Chem.* **1975**, *87*, 311.
(25) Hedman, B.; Frank, P.; Gheller, S. F.; Roe, A. L.; Newton, W. E.; Hodgson, K. O. *J. Am. Chem. Soc.* **1988**, *110*, 3798.
(26) Hedman, B.; Hodgson, K. O.; Solomon, E. I. *J. Am. Chem. Soc.* **1990**, *112*, 1643.
(27) Shadle, S. E.; Penner-Hahn, J. E.; Schugar, H. J.; Hedman, B.; Hodgson, K. O.; Solomon, E. I. *J. Am. Chem. Soc.* **1993**, *115*, 767.
(28) Shadle, S. E.; Hedman, B.; Hodgson, K. O.; Solomon, E. I. *Inorg. Chem.* **1994**, *33*, 4235.
(29) Shadle, S. E.; Hedman, B.; Hodgson, K. O.; Solomon, E. I. *J. Am. Chem. Soc.* **1995**, *117*, 2259.
(30) Glaser, T.; Hedman, B.; Hodgson, K. O.; Solomon, E. I. *Acc. Chem. Res.* **2000**, *33*, 859.
(31) Solomon, E. I.; Hedman, B.; Hodgson, K. O.; Dey, A.; Szilagyi, R. K. *Coord. Chem. Rev.* **2005**, *249*, 97.
(32) DeBeer George, S.; Brant, P.; Solomon, E. I. *J. Am. Chem. Soc.* **2005**, *127*, 667.
(33) Szilagyi, R. K.; Schwab, D. E. *Biochem. Biophys. Res. Commun.* **2005**, *330*, 60.
(34) DeBeer George, S.; Huang, K. W.; Waymouth, R. M.; Solomon, E. I. *Inorg. Chem.* **2006**, *45*, 4468.
(35) Delgado-Jaime, M. U.; Conrad, J. C.; Fogg, D. E.; Kennepohl, P. *Inorg. Chem. Acta.* **2006**, *359*, 3042.
(36) Pap, J. S.; Benedito, F. L.; Bothe, E.; Bill, E.; DeBeer George, S.; Weyhermuller, T.; Wieghardt, K. *Inorg. Chem.* **2007**, *46*, 4187.
(37) Adhikari, D.; Mossin, S.; Basuli, F.; Huffman, J. C.; Szilagyi, R. K.; Meyer, K.; Mindiola, D. J. *J. Am. Chem. Soc.* **2008**, *130*, 3676.
(38) Petersen, J. L.; Lichtenberger, D. L.; Fenske, R. F.; Dahl, L. R. *J. Am. Chem. Soc.* **1975**, *92*, 6433.
(39) Lauher, J. W.; Hoffmann, R. *J. Am. Chem. Soc.* **1976**, *98*, 1729.
(40) Caulettti, C.; Clark, J. P.; Green, J. C.; Jackson, S. E.; Fragala, I. L.; Ciliberto, E.; Coleman, A. W. *J. Electron Spectrosc. Relat. Phenom.* **1980**, *18*, 61.
(41) Bruce, M. R. M.; Kenter, A.; Tyler, D. R. *J. Am. Chem. Soc.* **1984**, *106*, 639.
(42) Zachmanoglou, C. E.; Docrat, A.; Bridgewater, B. M.; Parkin, G.; Brandow, C. G.; Bercaw, J. E.; Jardine, C. N.; Lyall, M.; Green, J. C.; Keister, J. B. *J. Am. Chem. Soc.* **2002**, *124*, 9525.
(43) Wang, X.; Chen, L.; Endou, A.; Kubo, M.; Miyamoto, A. *J. Organomet. Chem.* **2003**, *678*, 156.
(44) Casarin, M.; Finetti, P.; Vittadine, A.; Wang, F.; Ziegler, T. *J. Phys. Chem., A* **2007**, *111*, 5270.
(45) van Gisbergen, S. J. A.; Snijders, J. G.; Baerends, E. J. *Comput. Phys. Commun.* **1999**, *118*, 119.
(46) Fronzoni, G.; Stener, M.; Reduce, A.; Decleva, P. *J. Phys. Chem., A* **2004**, *108*, 8467.
(47) Ray, K.; DeBeer George, S.; Solomon, E. I.; Wieghardt, K.; Neese, F. *Chem.—Eur. J.* **2007**, *13*, 2783.
(48) Helmholz, L.; Kruh, R. F. *J. Am. Chem. Soc.* **1952**, *74*, 1176.

which had been secured to a Teflon block. After 48 h, the toluene had evaporated and the Teflon plate was removed, leaving a robust film fixed in the sample-plate window.

XAS Measurement. All data were measured at the Stanford Synchrotron Radiation Laboratory under ring conditions of 3.0 GeV and 60−100mA. Data were measured using the 54-pole wiggler beam line 6−2 in high magnetic field mode of 10 kG with a nickel-coated harmonic rejection mirror and a fully tuned (3150 eV) Si(111) double crystal monochromator. A chamber, similar to that previously described,[49] was used with the exception that the I_0 compartment was separated from the sample compartment by a 4.5 μm polypropylene film. The entire chamber, up to the beam pipe, was filled with helium, and the sample excitation fluorescence was measured against the incident beam using photodiode detectors. Data were collected at room temperature with four different step sizes such that energy steps of 3.73, 0.07, 0.61, and 3.87 eV were used between 2715.17−2805.19, 2805.19−2835.2, 2835.2−2905.21, and 2905.21−3350.31 eV, respectively. The energy was calibrated to 2820.20 eV using the maximum of the first pre-edge feature in the Cl K-edge XAS of the D_{2d}−Cs_2CuCl_4 standard, which was repeatedly analyzed in between sample scans.

Data Analysis. A first-order polynomial was fit to the pre-edge region, 2705.0−2805.8 eV, and then subtracted from the experimental data to eliminate the background of the spectrum. The data were normalized by fitting a first-order polynomial to the postedge region of the spectra, 2830.0−3350.31 eV, and setting the edge jump at 2836 eV to an intensity of 1.0. Fits to the Cl K-edges were performed using the program *IGOR 6.0* and a modified version of *EDG_FIT*.[50] Second-derivative spectra were used as guides to determine the number and position of peaks. Pre-edge and rising edge features were modeled by pseudo-Voigt line shapes and a step function. For the pre-edge and white line features, a fixed 1:1 ratio of Lorentzian to Gaussian contributions was used, and for the step function, a 1:1 ratio of arctangent and error function contributions was employed. Fits were performed over several energy ranges.

Results and Discussion

Cl K-edge Spectra of $(C_5H_5)_2MCl_2$. For ligand K-edge XAS measurements, samples are typically ground into a fine powder and thinly dispersed, to minimize self-absorption, on Cl-free Kapton tape.[25−37] Samples are prepared under an inert atmosphere and a thin polypropylene film, typically around 5 μm,[29] protects the samples from exposure to air. This technique is not suitable for use with radioactive materials, and we report an alternate method that involves dissolving a mixture of finely ground analyte powder with 3 μm polystyrene beads in toluene. The solution is transferred to slots in an aluminum sample holder, and the toluene is allowed to evaporate under a helium atmosphere, yielding the analyte encapsulated (essentially dissolved) in the polystyrene matrix. This procedure enables the analyte concentration to be rigorously controlled using standard analytical techniques, and, because the analyte and the polystyrene are both dissolved in toluene, the particle size and separation are minimized. Hence, as opposed to typical thin-film samples, the polystyrene encapsulation approach provides control over many factors that contribute to self-absorption.

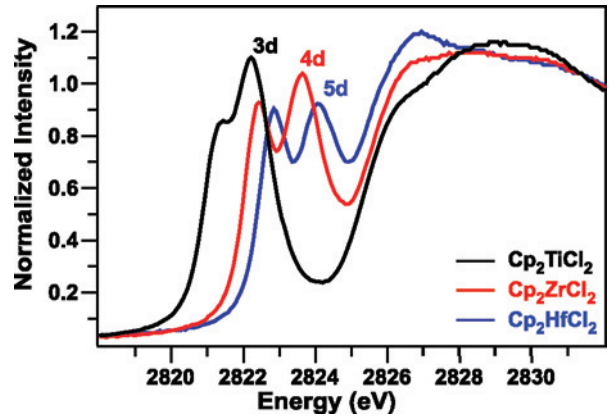

Figure 1. The Cl K-edge XAS for $(C_5H_5)_2MCl_2$ (M = Ti, black; Zr, red; Hf blue; **1**, **2**, and **3**, respectively) samples that were encapsulated in polystyrene.

Room temperature Cl K-edge XAS data were collected on samples of **1**−**3**, prepared as both thin films and in polystyrene matrices, at the Stanford Synchrotron Radiation Laboratory under helium atmospheres as fluorescence−excitation spectra using photodiode detectors (Figure 1 and Table 1). The energy was calibrated using the first pre-edge maximum of D_{2d}-Cs_2CuCl_4[48] fixed at 2820.20 eV.[51−53] Standard data reduction and analysis procedures were used and have been described elsewhere.[31] The spectral features of **1**−**3** were modeled using pseudo-Voigt line shapes with a fixed 1:1 Lorentzian to Gaussian ratio (Supporting Information). To study the minimization of self-absorption effects in the data, samples were analyzed using progressively decreasing analyte concentration until the observed intensity no longer varied. The optimum concentration appears to be at 0.8% by mass of analyte. For **1**−**3**, the polystyrene and thin-film spectral pairs are practically indistinguishable. For **1**, the spectra are essentially identical to the thin-film fluorescence spectrum reported by DeBeer George et al.,[32] and these results demonstrate that polystyrene encapsulation reproduces the thin-film intensities, with minimal self-absorption effects.

Figure 2 compares the normalized Cl K-edge pre-edge data and fits for the polystyrene films of **1**−**3**. The pre-edge features correspond to transitions from the Cl 1s orbitals to unoccupied MOs formed by interaction of the Cl 3p and M d orbitals, whereas the rising edge contains a Cl 1s to Cl 4p transition. The pre-edge peak energies and total intensities for **1**−**3** vary with increasing Z (Figure 2 and Table 1). For example, the spectrum for **1** contains two pre-edge features at 2821.19 and 2822.24 eV. These peaks move as a pair to 2822.37 and 2823.62 eV for **2** and 2822.82 and 2824.01 eV

(49) Shadle, S. E. Ph.D. Thesis, Stanford University, 1994.
(50) George, G. N., EDG_FIT, Stanford Synchrotron Radiation Laboratory, Stanford Linear Accelerator Center, Stanford University: Stanford CA, USA.
(51) Gewirth, A. A.; Cohen, S. L.; Schugar, H. J.; Solomon, E. I. *Inorg. Chem.* **1987**, *26*, 1133.
(52) Didziulis, S. V.; Cohen, S. L.; Gewirth, A. A.; Solomon, E. I. *J. Am. Chem. Soc.* **1988**, *110*, 250.
(53) Neese, F.; Hedman, B.; Hodgson, K. O.; Solomon, E. I. *J. Am. Chem. Soc.* **1999**, *38*, 4854.

Table 1. Comparison of Experimental and Calculated Pre-Edge Peak Energies (eV), intensities, and % Cl 3p Character[a] for $(C_5H_5)_2MCl_2$ Complexes (M = Ti, Zr, and Hf; **1**, **2**, and **3**, Respectively)

Compound	peak 1				peak 2				total			Peak Splitting (eV)	
	Energy (eV)	Int.	% Cl 3p	% Cl 3p	Energy (eV)	Int.	% Cl 3p	% Cl 3p	Int.	% Cl 3p	% Cl 3p		
	exptl	exptl	exptl	calcd	exptl	exptl	exptl	calcd	exptl	exptl	calcd	exptl	calcd
1 (thin film)[32]	2821.27	0.50	7	8	2822.29	1.24	18	13	1.74	25	21	1.02	
1 (thin film)	2821.20	0.47	7	6	2822.24	1.35	19	14	1.82	26	20	1.04	0.90
1 (polystyrene)	2821.19	0.44	6	6	2822.24	1.37	19	14	1.81	25	20	1.05	0.90
2 (thin film)	2822.46	0.54	8	6	2823.64	1.05	15	12	1.59	23	18	1.18	1.26
2 (polystyrene)	2822.37	0.65	9	6	2823.62	1.13	16	12	1.78	25	18	1.25	1.26
3 (thin film)	2822.98	0.54	8	6	2824.09	0.74	10	11	1.28	18	17	1.11	1.10
3 (polystyrene)	2822.82	0.65	9	6	2824.01	0.69	10	11	1.34	19	17	1.19	1.10

[a] The percent Cl 3p character is reported per M−Cl bond.

for **3**, which is consistent with the expected rise in energy for the 3d, 4d, and 5d orbital final states, respectively.

Using D_{2d}−Cs_2CuCl_4 as an intensity standard, with 7.5% Cl 3p character per Cu−Cl bond;[29,31,48,51–53] the Cl 3p character per M−Cl bond can be determined from curve fits for each metal complex. For polystyrene samples of **1**−**3**, the %Cl 3p character in the unoccupied metal-based orbitals was determined to be 25, 25, and 19%, respectively. These data are indistinguishable from the %Cl 3p character determined for the thin-film samples, which are 26, 23, and 18% for **1**−**3**, respectively, given the ca. 5% error associated with our measurement (Table 1). Both sets of data for **1** agree with the 25% Cl 3p character previously reported for the thin-film sample of $(C_5H_5)_2TiCl_2$, whose intensity was confirmed by a total electron yield measurement.[32] Hence, in addition to qualitative reproduction of thin-film Cl K-edge XAS data, polystyrene encapsulation can also be used to obtain quantitative data.

Electronic Structure Calculations on $(C_5H_5)_2MCl_2$. For a more detailed understanding of M−Cl bonding interactions, we conducted electronic structure calculations on $(C_5H_5)_2MCl_{2+}$ complexes using B3LYP hybrid density functional theory (DFT)[54] in the *Gaussian 03* code.[55] The Stuttgart 97 relativistic effective core potential and associated basis sets (minus the most diffuse function) were used for titanium, zirconium, and hafnium,[56] and the 6−31G* basis sets for carbon and hydrogen. For the chlorine atoms, the 6−31G* basis set was modified by recontracting the p functions to the B3LYP 2p through 6p atomic orbitals of Cl^{1-} (Supporting Information). The recontraction of the p space did not change the predicted structures and proved advantageous by providing a cleaner interpretation of the participating atomic orbitals in the molecular orbitals under consideration. These functionals and basis sets have been extensively tested for organometallic systems and have been shown to give good agreement with experimental data.[57–60] The populations of the Cl 3p orbitals of each compound were then obtained by Mulliken population analysis of each particular molecular orbital.

The electronic structure of bent metallocene dichlorides is well understood.[38–44] The bent $[(C_5H_5)_2M]^{2+}$ fragment is characterized by six M−(C_5H_5) orbital interactions at lower energy, leaving three low-energy metal orbitals ($1a_1$, $1b_2$, and $2a_1$) and two higher-lying metal orbitals ($1b_1$, $1a_2$) available to form bonding interactions with the Cl^{1-} ligands.[38–43] Whereas the first set of three orbitals is generally regarded as the most important for M−Cl bonding, all five

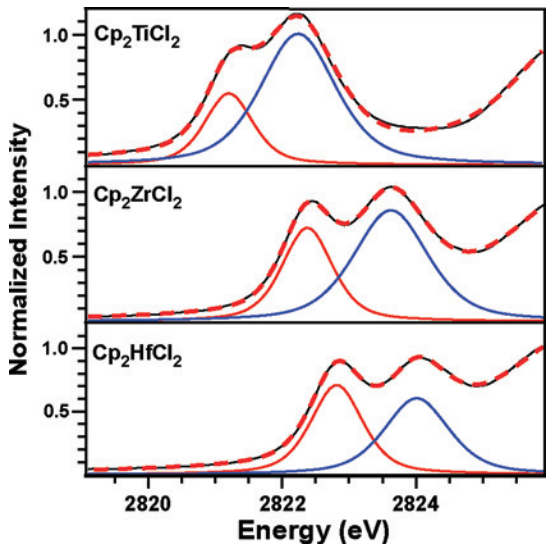

Figure 2. Cl K-edge XAS experimental data (black line), the curve fit (red dashes), and the pseudo-Voigt peaks used to generate the fit (red and blue lines) for the polystyrene film samples of $(C_5H_5)_2MCl_2$ (M = Ti, top; Zr, middle; Hf bottom; **1**, **2**, and **3**, respectively).

(54) Becke, A. D. *J. Chem. Phys.* **1993**, *98*, 5648.
(55) Frisch, M. J. ; Trucks, G. W.; Schlegel, H. B.; Scuseria, G. E.; Robb, M. A.; Cheeseman, J. R.; J.A. Montgomery, J.; Vreven, T.; Kudin, K. N.; Burant, J. C.; Millam, J. M.; Iyengar, S. S.; Tomasi, J.; Barone, V.; Mennucci, B.; Cossi, M.; Scalmani, G.; Rega, N.; Petersson, G. A.; Nakatsuji, H.; Hada, M.; Ehara, M.; Toyota, K.; Fukuda, R.; Hasegawa, J.; Ishida, M.; Nakajima, T.; Honda, Y.; Kitao, O.; Nakai, H.; Klene, M.; Li, X.; Knox, J. E.; Hratchian, H. P.; Cross, J. B.; Bakken, V.; Adamo, C.; Jaramillo, J.; Gomperts, R.; Stratmann, R. E.; Yazyev, O.; Austin, A. J.; Cammi, R.; Pomelli, C.; Ochterski, J. W.; Ayala, P. Y.; Morokuma, K.; Voth, G. A.; Salvador, P.; Dannenberg, J. J.; Zakrzewski, V. G.; Dapprich, S.; Daniels, A. D.; Strain, M. C.; Farkas, O.; Malick, D. K.; Rabuck, A. D.; Raghavachari, K.; Foresman, J. B.; Ortiz, J. V.; Cui, Q.; Baboul, A. G.; Clifford, S.; Cioslowski, J.; Stefanov, B. B.; Liu, G.; Liashenko, A.; Piskorz, P.; Komaromi, I.; Martin, R. L.; Fox, D. J.; Keith, T.; Al-Laham, M. A.; Peng, C. Y.; Nanayakkara, A.; Challacombe, M.; Gill, P. M. W.; Johnson, B.; Chen, W.; Wong, M. W.; Gonzalez, C.; Pople, J. A., *Gaussian*, Rev. D.01; Gaussian Inc.: Wallingford, CT, 2004.
(56) Kuchle, W.; Dolg, M.; Stoll, H.; Preuss, H. *J. Chem. Phys.* **1994**, *100*, 7535.
(57) Clark, A. E.; Martin, R. L.; Hay, P. J.; Green, J. C.; Jantunen, K. C.; Kiplinger, J. L. *J. Phys. Chem., A.* **2005**, *109*, 5481.
(58) Bi, S.; Lin, Z. *Organometallics* **2004**, *23*, 4882.
(59) Hay, P. J. *Organometallics* **2007**, *26*, 4424.
(60) Karttunen, V. A.; Linnolahti, M.; Pakkanen, T. A.; Maaranen, J.; Pitkanen, P. *Theo. Chem. Acc.* **2007**, *118*, 899.

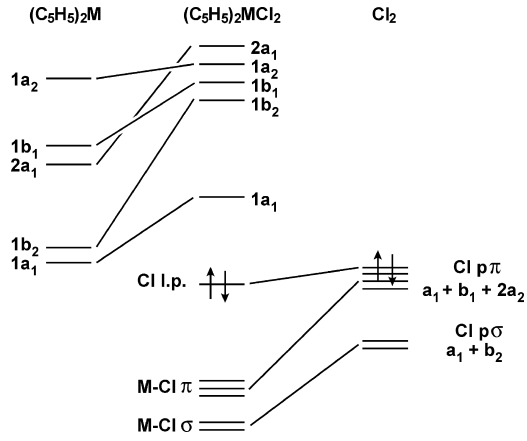

Figure 3. Qualitative MO interaction diagram showing the interaction of a $(C_5H_5)_2M$ fragment with Cl_2 to generate $(C_5H_5)_2MCl_2$.

are necessary to understand the XAS intensities due to a combination of σ and π orbital interactions with the Cl^{1-} levels at lower energy. A qualitative MO interaction diagram is shown in Figure 3. As a result of M−Cl bonding, the five resulting metal−based orbitals are all M−Cl antibonding and are shown in Scheme 2 (with the contributions from the $C_5H_5^{1-}$ ligands removed for clarity). The calculated orbital compositions are given in Table 2.

Comparison of the Experimental and Theoretical Cl K-Edge XAS. The first level of theory assumed that the transition amplitudes from the chlorine core levels to the virtual states were directly proportional to the %Cl p character of the virtual orbitals.[32] For all three compounds, our ground-state calculations suggest that the two lowest unoccupied orbitals in $(C_5H_5)_2MCl_2$ complexes are the $1a_1$ and $1b_2$ M−Cl antibonding orbitals. Hence, for **1**−**3** the first XAS pre-edge peak is attributed to a Cl 1s → $1a_1$ transition, which stems primarily from Cl 3p π-bonding with the metal $d_{x_2-y_2}$ orbital. Whereas it is tempting to assign the second pre-edge peak to a 1s → $1b_2$ transition, the calculations reveal that the $1b_2$ orbital is pushed sufficiently high in energy such that a manifold of four primarily metal *n*d molecular orbitals ($1b_2$, $1b_1$, $1a_2$, and $2a_1$) exist and are closely grouped together, spanning only 0.6, 0.9, and 1.1 eV for **1**−**3**, respectively.

Depending on the identity of the metal ion, all four of these metal d orbitals ($1b_2$, $1b_1$, $1a_2$, and $2a_1$) mix with the Cl 3p orbitals to varied extents with orbital mixing following the order Hf > Zr > Ti (Table 2). For example, in **1** the 1s → $1b_2$ transition contributes 87% to the total intensity of the second peak, whereas smaller contributions from the 1s → $1b_1$, $1a_2$, and $2a_1$ transitions provide the additional 13%. In contrast, the amount of metal Cl 3p/Hf 5d mixing is more evenly distributed in **3**, and the 1s → $1b_2$ transition accounts for only 56% of the total intensity of the second peak. These calculations are consistent with the experimental spectra for **1**−**3**, which show decreased amplitudes and increased peak widths for the second pre-edge features. Because the percent of Cl 3p character in the $1a_1$ molecular orbital was calculated and found experimentally to be the same for all three complexes, the differences in total covalency for the M−Cl bonds are attributable to the degree of Cl 3p orbital mixing with the $1b_2$, $1b_1$, $1a_2$, and $2a_1$ manifold of metal d orbitals, which decreases from **1** to **3**. This finding is similar to the trends revealed by gas-phase photoelectron spectroscopy of occupied orbitals in metallocene complexes.[14–24]

The ground-state calculations for the $(C_5H_5)_2MCl_2$ complexes show that as the principal quantum number increases, the total percent of $(C_5H_5)^{1-}$ orbital involvement also increases (Table 2). In contrast, the calculated 20, 18, and 17% Cl 3p character per M−Cl bond for **1**−**3**, respectively, decreases with increasing Z. Although, both theory and experiment suggest that the M−Cl bond for the 3d complex, **1**, is more covalent than the 5d analogue, **3**, the experimental comparison between the 3d and 4d complexes is obscured by the similar pre-edge intensities for **1** and **2**. For example, the %Cl 3p character in the M−Cl bond for **1** and **2** were experimentally indistinguishable for the polystyrene samples, whereas the thin-film samples indicate a decrease from 26 to 23% Cl 3p character for **1** to **2**, respectively. Given that the differences in the thin-film data are only slightly larger than the 5% experimental error, the calculations, which agree well with the experimentally determined values, provide additional insight and show 20% Cl 3p character in the M−Cl bond for **1** and 18% Cl 3p character for **2**. Hence, for **1**−**3** both experiment and theory indicate that the covalency of the M−Cl bond decreases on the order Ti > Zr > Hf and show that the differences between the 3d, 4d, and 5d group IV metallocenes are small in overall magnitude.

A more rigorous level of theory involves a linear response theory (TD-DFT) calculation,[61–63] where the probability amplitudes were extracted from the transition dipole moments between the calculated excited states and the ground states. The excitations originating from all of the intermediates states between the Cl 1s and the HOMO were not included so that only excitations from the core levels to virtual molecular orbitals could be analyzed. This allows the virtual orbitals to mix and reflect the presence of the core hole in chlorine. However, we do not include relaxations in the occupied orbitals associated with the core hole.[64]

Scheme 2

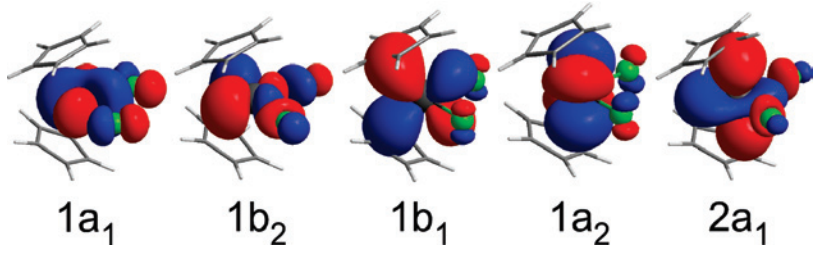

Table 2. Orbital Composition for the Five Metal d-Based Orbitals in $(C_5H_5)_2MCl_2$ (M = Ti, Zr, Hf; **1**, **2**, and **3**, Respectively)

	MO Label (Symmetry)					
	59($1a_1$)LUMO	60($1b_2$)	61($1b_1$)	62($1a_2$)	63($2a_1$)	Total
			$(C_5H_5)_2TiCl_2$, **1**			
energy (eV)	−2.80	−1.86	−1.81	−1.64	−1.44	
total % Ti 3d	77.6	57.1	72.5	70.1	73.4	350.7
total % Ti 4p	0.6	1	1	0	0	2.6
total % Cl 3p	12.1	17.2	2.2	1.4	6.3	39.2
total % $(C_5H_5)^{1-}$	9.7	24.7	24.3	28.5	20.3	107.5
			$(C_5H_5)_2ZrCl_2$, **2**			
energy (eV)	−2.23	−1.27	−0.98	−0.62	−0.34	
total % Zr 4d	69.9	43.8	73.2	67.4	77.9	332.2
total % Zr 5p	1	2.5	0	0	0	3.5
total % Cl 3p	12.2	10.8	2.7	3.9	6.5	36.1
total % $(C_5H_5)^{1-}$	16.9	42.9	24.1	28.7	15.6	128.2
			$(C_5H_5)_2HfCl_2$, **3**			
energy (eV)	−1.92	−1.00	−0.57	−0.17	0.14	
total % Hf 5d	65.3	38.6	69.3	61.5	81.3	316.0
total % Hf 6p	1.3	2.4	0.7	0	0	4.4
total % Cl 3p	11.2	8.0	2.6	4.2	7.8	33.8
total % $(C_5H_5)^{1-}$	22.2	51.0	27.4	34.3	10.9	145.8

Figure 4 compares the TD-DFT simulated Cl K-edge XAS with experimental XAS. The TD-DFT calculations reproduce the basic experimental features of peak intensity, peak area, and peak energies remarkably well, and provide additional confidence on spectral assignments.[57] The calculated and experimental spectra for **1**−**3**, Figure 4, show a decrease in amplitude and increase in peak width for the second pre-edge feature. The increase in width stems from the larger splitting among the d virtual states and the decrease in intensity to an overall reduction in oscillator strength, which is consistent with the calculated orbital compositions (Table 2). For the titanium system, our TD-DFT results and simulated spectra are in excellent agreement with recent spin−orbit relativistic TD-DFT simulations reported by Ziegler and co-workers.[44]

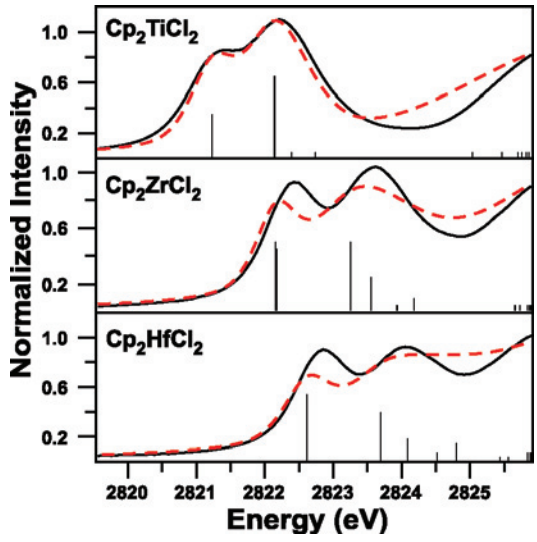

Figure 4. The Cl K-edge experimental data (red), the TD-DFT calculated spectrum (black), the TD-DFT calculated transitions (black bars) for polystyrene films of $(C_5H_5)_2MCl_2$ (M = Ti, top; Zr, middle, and Hf, bottom; **1**, **2**, and **3**, respectively). The height of the black bars represents the calculated oscillator strength for individual transitions.

Concluding Remarks

In summary, a quantitative analysis of the amount of Cl 3p involvement in M−Cl bonding for group IV metallocene dichlorides has been extended from $(C_5H_5)_2TiCl_2$ to $(C_5H_5)_2ZrCl_2$ and $(C_5H_5)_2HfCl_2$ using Cl K-edge X-ray Absorption Spectroscopy (XAS). These results demonstrate that the %Cl 3p character in the M−Cl bond decreases with increasing Z. Using ground-state DFT and TD-DFT calculations as a guide, we conclude that all five metal-based orbitals ($1a_1$, $1b_2$, $1b_1$, $1a_2$, and $2a_1$) must be considered when evaluating the M−Cl bonding in the group IV metallocene dichlorides. For **1**−**3**, the %Cl 3p orbital contribution to the $1a_1$ orbital did not appreciably change with Z, whereas the degree of chlorine involvement in the manifold of four higher-energy molecular orbitals — the $1b_2$, $1b_1$, $1a_2$, and $2a_1$ — decreased according to **1** > **2** > **3**. Taken together, it is clear that the covalency in M−Cl bonding is strongest for the first-row 3d metal center and decreases according to 3d > 4d > 5d.

It was also demonstrated that high-quality Cl K-edge XAS data obtained on traditional thin-film samples could be reproduced when analytes were encapsulated in a polystyrene matrix. Encouraged by these results and the application of DFT calculations to facilitate the analysis and interpretation of Cl K-edge XAS, it seems likely that polystyrene matrix encapsulation will afford a convenient method to safely contain radioactive samples to extend our studies to include actinide elements where both 5f and 6d orbitals are expected to play a role in M−Cl bonding and where transition assignments must rely on accurate theoretical calculations.

(61) Stratmann, R. E.; Scuseria, G. E.; Frisch, M. J. *J. Chem. Phys.* **1998**, *109*, 8218.
(62) Bauernschmitt, R.; Ahlrichs, R. *Chem. Phys. Lett.* **1996**, *256*, 454.
(63) Casida, M. E.; Jamorski, C.; Casida, K. C.; Salahub, D. R. *J. Chem. Phys.* **1998**, *108*, 4439.
(64) The absolute calculated transition energies show large errors due to the omission of atomic and extra-atomic relaxation associated with the core excitation,[64] relativistic stablization, and errors associated with the functional.[65] Hence, it was necessary to establish a constant shift of 64.9 eV for all calculated spectra.

Acknowledgment. The authors are grateful to E. I. Solomon and S. DeBeer George for helpful discussions. This work was supported at Los Alamos by the Division of Chemical Sciences, Geosciences, and Biosciences, Office of Basic Energy Sciences, US DOE, the, Glenn T. Seaborg Institute Postdoctoral fellowship (P.Y.), and Frederick Reines Postdoctoral Fellowship (S.A.K.). Portions of this research were carried out at the Stanford Synchrotron Radiation Laboratory, a national user facility operated by Stanford University on behalf of the U.S. Department of Energy, Office of Basic Energy Sciences. Los Alamos National Laboratory is operated by Los Alamos National Security, LLC, for the National Nuclear Security Administration of U.S. Department of Energy under contract DE-AC52-06NA25396.

Supporting Information Available: X-ray absorption spectra, structural parameters, and molecular orbitals. This material is available free of charge via the Internet at http://pubs.acs.org.

IC8004932

(65) Martin, R. L.; Shirley, D. A., Many-electron theory of Photoemission. In *Electron Spectroscopy, Theory, Techniques and Applications*; Academic Press: New York, 1977; Vol. 1, p 75.

(66) Tu, G.; Carravetta, V.; Vahtras, O.; Ågren, H. *J. Chem. Phys.* **2007**, *127*, 174110.